Electronic and Vibronic Coupling of the Special Pair of Bacteriochlorophylls in Photosynthetic Reaction Centers from Wild-Type and Mutant Strains of *Rhodobacter Sphaeroides*

E. T. Johnson,[†] F. Müh,[‡] E. Nabedryk,[§] J. C. Williams,[||] J. P. Allen,[||] W. Lubitz,[⊥] J. Breton,[§] and W. W. Parson*,[†]

Department of Biochemistry, Box 357350, University of Washington, Seattle, Washington 98195-7350, Institut für Experimentalphysik, Freie Universität Berlin, Arnimallee 14, D-14195 Berlin, Germany, Service de Bioénergétique, CEA Saclay, Bât 532, F-91191 Gif Sur Yvette Cedex France, Department of Chemistry and Biochemistry, Arizona State University, Tempe, Arizona 85287, and Max-Planck-Institut für Strahlenchemie, Stiftstr. 34−36, D-45470 Mülheim/Ruhr, Germany

Received: April 22, 2002; In Final Form: September 9, 2002

The photosynthetic reaction center (RC) is an integral membrane protein that carries out the initial charge-separation reactions of photosynthesis. Upon light excitation, a pair (P) of bacteriochlorophylls (Bchls) donates an electron to a bacteriopheophytin (H_L), generating an ion-pair state ($P^+H_L^-$). Previous ENDOR studies of RCs from the purple bacterium *Rhodobacter sphaeroides* have shown that the unpaired electron of P^+ is distributed unequally between the two Bchls of P, with about 2/3 of the unpaired spin and positive charge residing on the Bchl bound to subunit L (P_L) and 1/3 on the Bchl bound to M (P_M). To investigate the protein's role in establishing the energies of the cations P_L^+ and P_M^+ through long-range electrostatic interactions, we mutated Arg L135 and Arg M164 individually to Leu or Glu and measured the effects on the Special TRIPLE and FTIR spectra of P^+. These highly conserved residues occupy homologous positions on either side of P but have no hydrogen bonds or steric interactions with the pigments. Previous work has shown that replacing Arg by Leu at either site lowers the midpoint potential (E_m) of P/P^+ by about 15 mV; replacing it by Glu lowers the E_m by about 35 mV. We found that the mutations also alter the spin distribution in P^+. The mutation R(L135)E stabilizes P_L^+ relative to P_M^+, increasing the ratio of the spins to 3.1, whereas R(M164)E decreases the spin ratio to 1.3. Replacing R(L135) or R(M164) by Leu gave spin ratios of 2.9 or 1.6, respectively. FTIR measurements showed that the mutations also affect the vibrational spectra of P and P^+ and the electronic transition between the eigenstates of P^+. The R(L135)E mutation increases the splitting between the keto C═O stretching bands of P_L^+ and P_M^+, whereas the R(M164)E mutation decreases this splitting. The changes in the keto frequency are correlated with calculated changes in the projection of the local electric field along the C═O bond, and give a Stark tuning rate in the range 0.81−1.45 cm^{-1}/(MV/cm). Cooling the RCs to 100 K during illumination increases the splitting between the keto bands of P_L^+ and P_M^+ in wild-type and R(L135)E RCs and shifts the electronic transition to higher energies, suggesting that relaxations of the protein further stabilize P_L^+ relative to P_M^+. Fitting the electrochemical, ENDOR, and FTIR data to a self-consistent molecular orbital model required including both vibronic and electronic coupling of P_L^+ and P_M^+ and yielded an electronic coupling constant of approximately −155 meV and a reorganization energy of approximately 220 meV.

Introduction

The initial steps of charge separation in photosynthetic organisms occur in a pigment−protein complex called the reaction center (RC). Reaction centers from purple photosynthetic bacteria typically contain three protein subunits (L, M, and H), four bacteriochlorophyll (Bchl) molecules, two bacteriopheophytins (Bphe), two quinones, a nonheme iron, and one carotenoid (see ref 1 for a recent review). Two of the Bchls (P_L and P_M) form a tightly coupled dimer (P) that serves as the primary electron donor. Upon excitation with light, P transfers an electron to one of the Bphes (H_L) by way of one of two "accessory" Bchls (B_L). The reduced Bphe then passes an electron to a quinone (Q_A).

P_L and P_M are located on either side of a 2-fold rotational axis of noncrystallographic symmetry.[2−5] A 180° rotation around this axis approximately interchanges corresponding atoms of the Bchls, along with the positions of homologous residues in the L and M polypeptides. The two accessory Bchls, the pair of Bphes, and to a lesser extent the two quinones also are arranged in symmetrical branches on opposite sides of the rotation axis. The charge-separation reactions, however, are strongly asymmetrical, with electron transfer to B_L and H_L occurring much more rapidly than transfer to their counterparts B_M and H_M in the opposite branch.[6−9] The high specificity of this process appears to depend in part on the energies of the ion pairs $P^+H_L^-$ and $P^+B_L^-$, which are controlled largely by

* To whom correspondence should be addressed.
[†] University of Washington.
[‡] Freie Universität Berlin.
[§] Service de Bioénergétique.
[||] Arizona State University.
[⊥] Max-Planck-Institut für Strahlenchemie.

10.1021/jp021024q CCC: $22.00
Published on Web 10/23/2002

electrostatic interactions with the protein. The factors that create the electrostatic asymmetry have been explored by site-directed mutagenesis[10−13] and computational approaches[14−16] but remain only partially understood.

The oxidized electron donor (P^+) can be viewed as an electronically coupled system of two Bchls with basis states $|P_L^+\rangle$ and $|P_M^+\rangle$, in which the positive charge and the unpaired electron spin are localized entirely on either P_L or P_M.[17−25] In this model, stationary ground and excited states of P^+ ($|\gamma_+\rangle$ and $|\gamma_-\rangle$) are constructed from linear combinations of $|P_L^+\rangle$ and $|P_M^+\rangle$ with coefficients that depend on an electronic coupling strength (β) and the difference between the energies of the basis states (δ). The ratio of the net spins on P_L and P_M in the ground state (ρ_L/ρ_M) has been measured experimentally from the ENDOR and Special TRIPLE spectra of P^+.[26−28] In RCs from wild-type *Rhodobacter sphaeroides*, ρ_L/ρ_M was found to be 2.1.[26] The ratio of the net positive charges on the two molecules is assumed to be essentially the same as ρ_L/ρ_M, although the spin and charge distributions are not strictly identical.[29,30] A broad absorption band in the region of 2700 cm^{-1} has been assigned to transitions between $|\gamma_+\rangle$ and $|\gamma_-\rangle$ and has been studied by FTIR spectroscopy.[17,24,25,31,32]

The electronic model for P^+ has been investigated by making site-directed mutations that add or remove hydrogen bonds to P_L or P_M. Each such hydrogen bond increases the midpoint potential (E_m) of P/P^+ by approximately 50 mV and combinations of hydrogen bonds can shift ρ_L/ρ_M over the range 0.28−4.94.[28,33] These results have been explained by assuming that adding a hydrogen bond to the 13^1-keto carbonyl of P_L or P_M selectively destabilizes either $|P_L^+\rangle$ or $|P_M^+\rangle$, respectively, without changing β (see refs 23 and 34 for the IUPAC numbering of Bchl *a*).

In an extension of this work, Artz et al.[21] described a set of mutations that replaced Leu M160, a residue within H-bonding distance to the oxygen of the 13^1-keto group of P_M, by eight different amino acids. All of the mutations made the spin distribution more asymmetric and increased the E_m, as expected if the hydrogen bond destabilizes $|P_M^+\rangle$ or, in an alternate view, stabilizes the HOMO of P_M. In general, residues with side chains that could approach the 13^1-keto oxygen more closely had larger effects. The L(M160)H mutation had the largest effect, increasing ρ_L/ρ_M to 5 and raising the E_m by 60 mV. The asymptotic value for the E_m when $|P_M^+\rangle$ is destabilized so severely that the charge resides exclusively on P_L should be proportional to the ionization potential of P_L and is estimated to be 650 mV relative to the standard hydrogen electrode at pH 7.[22,23] This is comparable to the E_m of 640−660 mV measured in "heterodimer" mutants, in which P_M is replaced by a Bphe and the positive charge of P^+ localizes strongly on P_L.[35] Fitting the E_m values and the spin ratios to the orbital model gave a value of $|\beta|$ in the range 170−240 meV (1400−1900 cm^{-1})[21] or about 180 meV (1450 cm^{-1}) after a correction to one of the equations.[22,23] However, the electronic model with $|\beta| = 190$ meV implies that a hydrogen bond from a histidine at M160 destabilizes $|P_M^+\rangle$ by 220 meV. This is a much larger effect than the 80 mV change in E_m observed for the corresponding hydrogen bond to P_L in the L(L131)H mutation in the H(M202)L heterodimer.[35] Moreover, a recent analysis of additional data from similar mutations at position L131 showed that a simple electronic coupling model using a single value for β could not fit the data from both the L131 and M160 mutations.[23]

The effects of some of the other hydrogen-bonding mutants that have been described also have been difficult to interpret. The mutation H(L168)F removes a hydrogen bond from the 3^1-acetyl oxygen of P_L, which would be expected to stabilize $|P_L^+\rangle$ and thus lower the E_m and increase both ρ_L/ρ_M and the energy of the 2700 cm^{-1} transition. This mutation does lower the E_m,[36] but it decreases ρ_L/ρ_M to less than 1[28] and shifts the FTIR transition to lower energies.[37] The mutation F(M197)H introduces a hydrogen bond to P_M that should destabilize $|P_M^+\rangle$ and thus increase the E_m, ρ_L/ρ_M and the energy of the 2700-cm^{-1} band. This mutation raises the E_m,[38] but again, it decreases ρ_L/ρ_M slightly and lowers the energy of the 2700 cm^{-1} band (Nabedryk, E., Wachtveitl, J., Gray, K. A., Oesterhelt, D., Breton, J. Unpublished results). On the other hand, the mutation F(M197)Y increases both the E_m and ρ_L/ρ_M as expected.[39−41] These observations suggest that some of the H-bond mutations affect parameters other than simply the energy difference between $|P_L^+\rangle$ and $|P_M^+\rangle$. They could, for example, perturb the molecular orbitals of one or both Bchls by reorienting the acetyl groups,[42] which could change both the energies of the basis states and the electronic coupling strength.

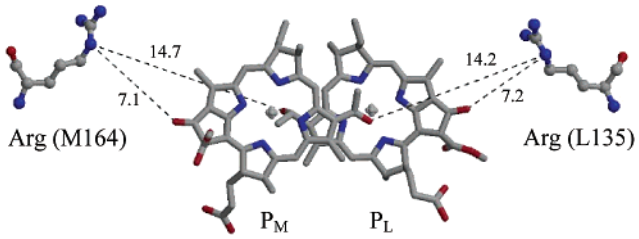

Figure 1. Locations of Arg L135 and Arg M164 relative to P_L and P_M in the crystal structure of *Rb. sphaeroides* RCs.[5] The distances (Å) from the Arg N_η atoms to the 13^1-keto oxygen of the closer Bchl and the 3^1-acetyl oxygen of the more distant Bchl are indicated. The distances from N_η of Arg L135 to the Mg atoms of P_L and P_M are 12.5 and 19.7 Å, respectively; N_η of Arg M164 is 13.1 Å from the Mg of P_M and 20.1 Å from that of P_M.

In the current work, we have mutated residues that do not interact directly with the pigments. We focused on arginines L135 and M164, which are the closest ionizable residues to P in the *Rb. sphaeroides* RC but are too far away to form hydrogen bonds to either P_L or P_M. The guanidino N_η atom of each of these residues is about 7 Å from the 13^1-keto oxygen of the Bchl attached to the same subunit and about 14 Å from the 3^1-acetyl oxygen of the other Bchl (see Figure 1). Replacing Arg L135 or M164 by a neutral or anionic residue thus should shift the energies of $|P_L^+\rangle$ and $|P_M^+\rangle$ through long-range electrostatic interactions, with relatively little effect on β. We have measured the effects of these mutations by the changes in the E_m[43] and the Special TRIPLE and FTIR difference spectra of P^+ and have attempted to account for the results in the framework of a model that includes both electronic and vibronic coupling.

The mutant RCs described here also provide insight into relaxations of the protein that stabilize $P^+Q_A^-$, the product of photochemical charge separation. Light-induced charge separation at room temperature causes dark-adapted RCs to relax to a light-adapted conformation that can be trapped by freezing the RCs during illumination.[44−46] One indication of this relaxation is a change in the $P^+Q_A^-$ recombination kinetics. If RCs are cooled in the dark, the recombination following excitation at 77 K is fit well by a single exponential with a time constant of 25 ms. In RCs that are illuminated during cooling, the kinetics become disperse and the mean time constant increases to about 120 ms. The dark-adapted state can be regenerated by warming the RCs to room temperature and recooling in the dark. Kleinfeld et al.[44] suggested that the changes in the recombination kinetics could be explained by a

5% increase in the distance between P^+ and Q_A^- in RCs that were cooled in the light. More recently, McMahon et al.[45] have shown that the nonexponential kinetics could result from a distribution of energy gaps and electronic couplings between P and Q_A. However, the molecular details of the protein relaxation have remained unclear. We have investigated the protein relaxation around $P^+Q_A^-$ by comparing the FTIR difference spectra of RCs cooled in the dark or under illumination. Some of the spectral differences resemble changes caused by the R(L135)E mutation, suggesting that they reflect an increased electrostatic stabilization of P_L^+ relative to P_M^+.

Methods

Construction and Purification of Mutant RCs. Oligonucleotide-mediated site-directed mutagenesis was accomplished with the Chameleon Kit (Stratagene) for the mutations of Leu and Glu at both R(L135) and R(M164). The mutagenesis was performed in pUC18 or pUC19 vectors containing portions of the L or M subunits, following methods developed by Williams et al.[33,47,48] After transformation into *Escherichia coli* strain DH5α cells and purification of the mutated plasmid DNA, the regions containing the mutations were subcloned into the *puf* operon. The R(M164) mutations were cloned into the pRKSCH vector.[48] The R(L135) mutations were cloned into the pRKSCH/pHis vector, which contains a tail of seven histidine residues at the carboxyl terminal of the M subunit.[49] The plasmids were transformed into the *E. coli* strain S-17 and conjugated with ΔLM1.1, a *Rb. sphaeroides* strain that has the RC deleted.[47] DNA from the mutant strains was purified and sequenced to ensure that the mutations had been introduced correctly.

Wild-type and mutant *Rb. sphaeroides* strains were grown semiaerobically in rich media for 3−5 days in the dark.[47] RCs from the R(M164) mutants were isolated by standard procedures[28,50] with minor modifications. The solubilization of the RCs was achieved with 0.65% *N*,*N*-dimethyldodecylamine-*N*-oxide (LDAO, Fluka), which is slightly lower than the 1.2% used by Feher and Okamura.[50] After ultracentrifugation, the supernatant was brought to 1% LDAO and 30% NH_4SO_4 (wt/vol) to precipitate the RCs. The Celite step was omitted, and the solubilized floating pellet was dialyzed to remove salts and loaded onto a DEAE column. The RCs were eluted with a gradient of 0.03−0.25 M NaCl. RCs from the R(L135) mutations were isolated using a protocol that exploited the histidine tag[49] and were purified further by chromatography on DEAE-sepharose (Bio-Rad). The purified RCs were dialyzed against 15 mM Tris pH 8, 0.025% LDAO, and 1 mM EDTA and concentrated to an OD_{805} of 40 in a 1 cm cuvette using an Amicon pressure cell or a Centricon-50 filter device (Amicon). The purity of the sample was measured by the ratio OD_{280}/OD_{805} and typically was between 1.4 and 1.8. The RCs with R(L135) mutations were significantly less stable than those with mutations of R(M164), as judged by changes in the absorption spectrum during dialysis at 4 C. Measurements of the E_m of P/P^+ in the mutant RCs have been described elsewhere.[43]

RCs solubilized in the detergent LDAO have been shown to have two stable conformations with different ρ_L/ρ_M ratios.[51] To ensure that the RCs were in the conformation that absorbs at longer wavelengths, LDAO was replaced by the detergent CHAPS. A concentrated solution of CHAPS was added directly to a dialysis bag containing the RCs to give 2 mM CHAPS, and the detergent exchange was completed by equilibrium dialysis overnight against 2 mM CHAPS, 15 mM Tris pH 8.0, and 1 mM EDTA. The RCs then were concentrated to an $OD_{805} \sim 100$ using centricon 50 filters (Amicon).

Special TRIPLE Spectroscopy. Special TRIPLE spectra were recorded at 288 K on a Bruker ESP 300E spectrometer with a home-built cavity and ENDOR/TRIPLE accessories as described.[23,27,28] P^+ was obtained by continuous illumination of the sample with saturating light from a 100 W tungsten halogen lamp filtered through 7 cm of water to reduce the light intensity for wavelengths greater than 1000 nm and glass filters to cut off light for wavelengths less than 600 nm.[23] Because multiple TRIPLE resonances overlap, deconvolution of the spectra is necessary to fit the individual bands.[52]

FTIR Spectroscopy. Light-induced FTIR difference spectra of hydrated films were recorded with a Nicolet 60SX FTIR spectrometer equipped with a MCT-A detector, a KBr beam splitter, and a cryostat.[53,54] Between 100 and 1000 cycles of dark and light spectra were averaged to produce each final spectrum. Each FTIR measurement cycle required about 45 s, consisting of 12 s in the dark, 12 s in slightly subsaturating continuous light, a second 12 s period in the dark, and about 9 s calculation time with the sample in darkness. The RC films were cooled to 100 K either in the dark or during continuous illumination, allowing the protein to freeze in conformations that preferentially stabilized either PQ_A or $P^+Q_A^-$, respectively.[55] Electron transfer to Q_B was inhibited by 1 mM stigmatellin. Because the FTIR spectra above 3000 cm^{-1} are distorted by water absorption, we also prepared less hydrated ("dry") films of RCs.[17] The difference spectra were normalized by scaling all of the spectra so that the region near the small, negative Q_A absorption band at 1604 cm^{-1} was constant.[56]

Results

Effects of the Arg Mutations on the Spin Distribution in P^+. To examine the effects of the mutations on the distribution of electron spin and charge in P^+, we measured the Special TRIPLE spectra of photochemically oxidized RCs at 288 K. Figure 2 shows the spectra obtained with wild-type, R(L135)L, R(L135)E, R(M164)L, and R(M164)E RCs. The hydrogens of methyl groups 2^1 and 12^1 give prominent ENDOR signals that have been assigned by selective deuteration and comparisons to other known systems.[23,57−59] (Methyl 2^1 is attached to Bchl ring A and 12^1 to ring C.) With the radical cation of monomeric Bchl in solution, the isotropic hyperfine coupling constants (hfcs) for these hydrogens are proportional to the unpaired electron π-spin densities on carbons 2 and 12.[60,61] The situation in P^+ is more complicated because the spin is distributed between P_L and P_M. Previous work has shown that, in wild-type RCs, the hfcs for the methyl hydrogens of P_L ($A(2^1_L)$ and $A(12^1_L)$) are larger than the corresponding hfcs of P_M ($A(2^1_M)$ and $A(12^1_M)$), demonstrating that the spin is divided unequally in favor of P_L. Assuming that the π molecular orbitals of P_L and P_M are similar and that the methyl proton hfcs of each Bchl scale with the spin population, the ratio of the spins of P_L and P_M can be evaluated as

$$\frac{\rho_L}{\rho_M} = \frac{A(2^1_L) + A(12^1_L)}{A(2^1_M) + A(12^1_M)} \quad (1)$$

This same expression should give approximately the ratio of the net positive charges on the two molecules (see Discussion in ref 23).

The spectra of the L135 mutants were slightly noisier than those of the M164 mutants or wild-type RCs, possibly because of the greater instability of the RCs. However, deconvolution of the spectra[52] yielded reasonable hfcs (Table 1). The results

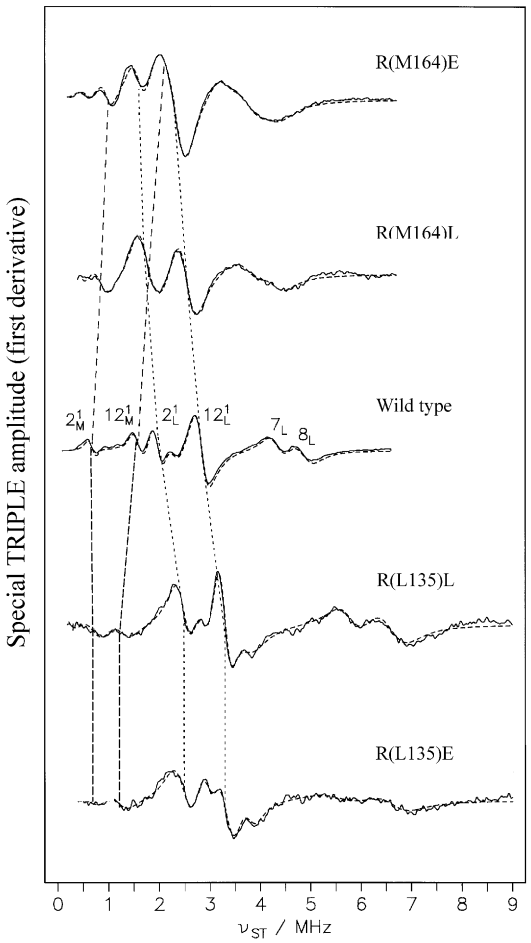

Figure 2. ^{1}H Special TRIPLE spectra of P^+ in wild-type *Rb. sphaeroides* RCs and the R(L135) and R(M164) mutants. The measured spectra are shown with solid lines; fitted spectra, with short-dashed lines. The resonances assigned to protons in methyl groups 2^1 and 12^1 of P_L are indicated by dotted lines, and those of the corresponding protons in P_M are indicated by long-dashed lines. The resonance frequencies (ν_{ST}) correspond to half the hyperfine coupling constants. Experimental conditions: temperature, 288 K; rf power, 2 × 150 W; microwave power, 10−20 mW; rf modulation depth, 150 kHz (frequency 12.5 kHz). Each spectrum is an average of 50−100 scans.

for wild-type RCs are in agreement with previous measurements.[23,27,28,51] In the M164 mutants, the Special TRIPLE features assigned to $|P_L^+\rangle$ shift to lower frequencies, whereas those assigned to $|P_M^+\rangle$ shift upward. In the L135 mutants, the features assigned to $|P_L^+\rangle$ shift to higher frequencies, whereas those of $|P_M^+\rangle$ are more difficult to resolve but evidently shift downward. The changes in the ratios of the hfcs for P_L and P_M indicate that the mutations at M164 make the dimer more symmetric, presumably by stabilizing $|P_M^+\rangle$ relative to $|P_L^+\rangle$. The calculated spin ratio ρ_L/ρ_M decreases from 2.1 in wild-type RCs to 1.6 and 1.3 in the Leu and Glu mutants, respectively. The L135 mutations have the opposite effect, stabilizing $|P_L^+\rangle$ and making the spin distribution more asymmetric. Here, ρ_L/ρ_M increases to 2.9 and 3.1 in the Leu and Glu mutations, respectively.

The ratios $R_{L,M} = \{A(12^1_{L,M})\}/\{A(2^1_{L,M})\}$ and sums $\Sigma = A(2^1_L) + A(12^1_L) + A(2^1_M) + A(12^1_M)$ provide probes of the intramolecular spin distributions, which could reveal effects of the mutations on the molecular orbitals of the individual Bchls.[23,28] As shown in Table 1, R_L and R_M are nearly unchanged in the M164 mutants. R_M may be somewhat smaller in the L135 mutants, but is less well determined here because the $A(2^1_M)$ resonances are not well resolved (see Figure 2). A comparable change in R_L occurs in the H(M202)L heterodimer mutant and could reflect localization of the spin on a single Bchl.[28,62]

TABLE 1: Hyperfine Coupling Constants for P^+ in Wild-Type and Mutant RCs[a]

strain	R(M164)E	R(M164)L	wild-type	R(L135)L	R(L135)E
$A(12^1_L)$	4.8	5.1	5.70	6.6	6.6
$A(2^1_L)$	3.2	3.4	3.96	5.0	5.0
$A(12^1_M)$	4.3	3.8	3.20	2.6	2.4
$A(2^1_M)$	1.9	1.7	1.37	1.4	1.3
$A(\beta)$	8.4	8.6	9.70	13.2	13.2
	7.5	7.6	8.70	11.6	11.4
	6.7		6.25	7.2	7.6
	1.2		4.50	5.8	5.9
R_L	1.5	1.5	1.44	1.3	1.3
R_M	2.3	2.2	2.34	1.9	1.8
Σ	14.2	14.0	14.23	15.6	15.3
ρ_L/ρ_M	1.3	1.6	2.11	2.9	3.1
ρ_L	0.56	0.61	0.68	0.74	0.76

[a] $A(12^1)$ and $A(2^1)$ are the isotropic ^{1}H hyperfine coupling constants (hfcs, in MHz) for the protons of methyl carbons 12^1 and 2^1; subscript L or M denotes P_L or P_M. The $A(\beta)$ are the hfcs assigned to Bchl β protons, which were included in the fitted spectra in Figure 2 but were not used in the calculations of spin distributions (see ref 34 for a definition of β protons). The estimated errors of the hfcs are ±0.03 MHz for wild-type RCs and ±0.1 MHz for the mutants. R_L, R_M, Σ, ρ_L, and ρ_L/ρ_M are defined in the text. The uncertainty in the spin ratios (ρ_L/ρ_M) is approximately 0.1.

Effects of the Mutations on the P^+/P Vibrational Difference Spectrum. Vibrational spectroscopy has been used extensively to explore the Bchls and the surrounding protein in the RC. Changes in the vibrational spectrum associated with the oxidation of P can be obtained by subtracting the FTIR spectrum of a sample in the dark (PQ_A) from the spectrum of the same sample under continuous illumination ($P^+Q_A^-$). $P^+Q_A^-/PQ_A$ difference spectra obtained in this manner have positive and negative peaks that reflect, respectively, $P^+Q_A^-$ and PQ_A absorption. Oxidation of P causes changes in many vibrational modes, some of which have been assigned by comparison to the spectra of Bchl in solution and from the effects of isotopic substitutions and site-directed mutagenesis.[53,63−66] The 13^1-keto C═O stretching modes of $|P_L^+\rangle$ and P_L in wild-type RCs have been assigned to bands at 1713 and 1693 cm^{-1}, respectively, and those of $|P_M^+\rangle$ and P_M have been assigned to 1703 and 1683 cm^{-1}.[53] The 13^3-ester carbonyl absorbs at 1753 and 1747 cm^{-1}, but the contributions from the two Bchls here are not resolved.[65] The absorption bands of the 3^1-acetyl groups of P_L and P_M are shifted relative to one another because of differences in hydrogen bonding. In wild-type *Rb. sphaeroides*, the acetyl of P_L is hydrogen bonded to His L168 and absorbs in the region of 1620 cm^{-1}, whereas the free acetyl of P_M absorbs near 1650 cm^{-1}.[67−70] The acetyl bands are difficult to see in $P^+Q_A^-/PQ_A$ FTIR difference spectra because of overlapping contributions in the 1620−1660 cm^{-1} range from peptide and quinone C═O modes. Features attributable to Q_A^- or Q_A can be identified in the $P^+Q_A^-/PQ_A$ difference spectra but usually are less prominent than those associated with the Bchls.

Figure 3 shows $P^+Q_A^-/PQ_A$ FTIR difference spectra in the region 1800−1200 cm^{-1} for the wild-type and several mutant RCs at 100 K. Spectra of RCs that were cooled in the dark are in the upper panel, and spectra of RCs cooled under continuous illumination are in the lower. The clearest effects of the mutations are on the keto C═O vibrations in the region of 1700−1720 cm^{-1}, probably because the 13^1-keto oxygen atoms are on the edges of the Bchls closest to the mutation sites and

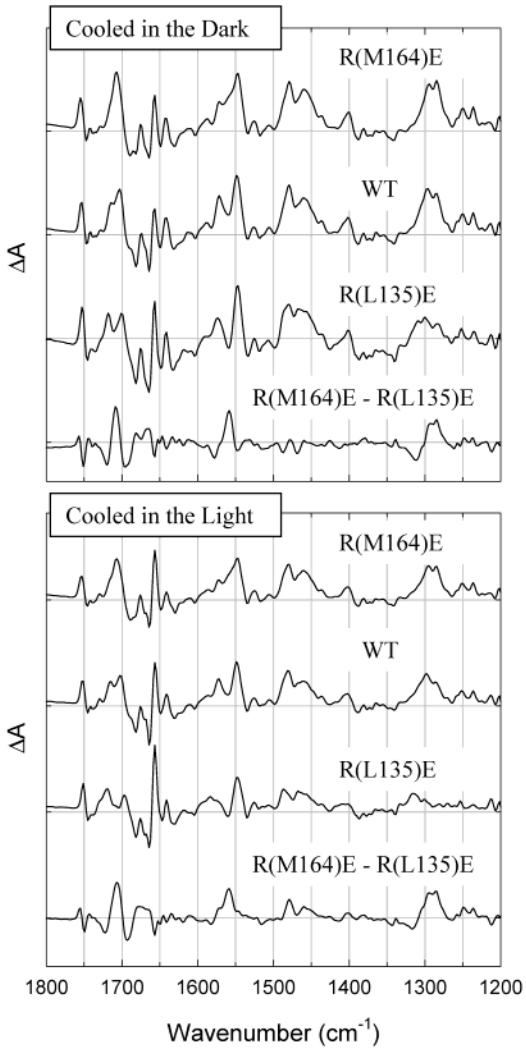

Figure 3. $P^+Q_A^-/PQ_A$ (light *minus* dark) FTIR difference spectra of RCs in hydrated films that were cooled to 100 K in the dark (*top panel*) or light (*bottom*). The $P^+Q_A^-/PQ_A$ double-difference spectra between R(M164)E and R(L135)E is also shown. The spectra are normalized in the Q_A band at 1604 cm^{-1}. These spectra are expansions of the region between 1200 and 1800 cm^{-1} from the spectra shown in Figure 5.

thus experience the largest changes in local electric field (see below). The R(L135)E mutation strengthens the higher-energy $|P_L^+\rangle$ band relative to the $|P_M^+\rangle$ band at lower energies and moves the peaks apart to 1718 and 1700 cm^{-1} (see Figure 3 and Table 2). In R(M164)E, by contrast, the P^+ absorption coalesces into a single band at 1707 cm^{-1} with a weak shoulder on the high-energy side. These features of the spectra are consistent with a shift of the spin distribution toward P_L in the L135 mutants and toward P_M in the M164 mutants. The two absorption bands of P in the region of 1680−1695 cm^{-1} also have more equal strengths in the R(M164)E mutant. The effects of replacing Arg L135 or M164 by Leu were qualitatively similar to those of the Glu mutations (not shown).

The FTIR spectra of the R(L135)E, wild-type, and R(M164)E RCs also differ in the intensities of bands in the regions of 1290, 1480, and 1560 cm^{-1} (see Figure 3). These bands have been attributed to "phase-phonon" vibrational modes that are formally forbidden by symmetry in monomeric Bchl but become allowed by coupling to the electronic transition between ground and excited eigenstates of P^+.[19,25,71] The phase-phonon bands are weakened in the R(L135)E mutant relative to wild-type RCs and are slightly enhanced in the R(M164)E mutant. This is consistent with the mutations' effects on the strength of the electronic transition of P^+, as discussed below.

TABLE 2: 13^1-Keto Vibration Energies in Wild-Type and Mutant RCs Cooled in the Dark or in the Light

	cooled in the dark[a] (cm^{-1})				cooled in the light[b] (cm^{-1})			
strain	P_L^+	P_M^+	P_L	P_M	P_L^+	P_M^+	P_L	P_M
R(M164)E	1707	1707	1691	1682	1707	1707	1689	1684
WT	1713	1703	1692	1682	1715	1702	1692	1682
R(L135)E	1718	1700	NR[c]	1682	1720	1697	NR	1682

[a] Hydrated films cooled in the dark. [b] Hydrated films cooled in the light. [c] Not resolved.

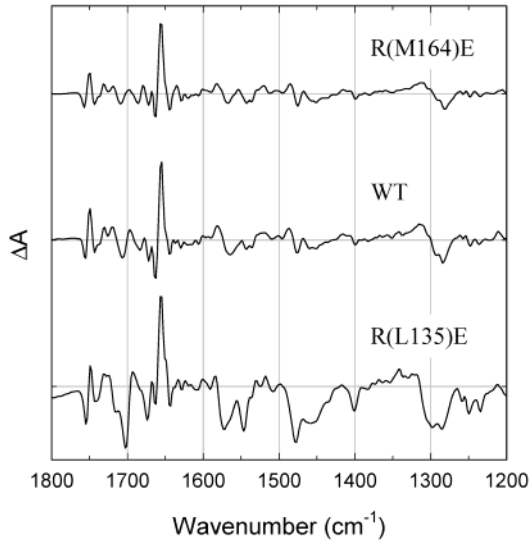

Figure 4. $P^+Q_A^-/PQ_A$ double-difference spectra between hydrated films of RCs cooled to 100 K in the light or dark. Positive peaks indicate larger absorbance increases (P^+ absorption) for RCs cooled in the light. The corresponding single-difference spectra are shown in Figure 3.

The arginine mutations cause only minor changes in the frequency of other carbonyl vibrations. The ester vibrations near 1750 cm^{-1} are nearly identical to those measured in the wild-type, displaying only a small shift of both the negative and the positive components to higher energy in R(M164)E compared to R(L135)E (see Figure 3). The changes in the acetyl C═O vibrations in the region 1620−1650 cm^{-1} are too small to interpret with confidence.

Illuminating the RCs during cooling allows the protein to relax around the charge-separated state, $P^+Q_A^-$.[44,55] The effects of this relaxation on the FTIR difference spectra in the carbonyl region can be seen by comparing the upper and lower panels of Figure 3. Figure 4 shows double difference spectra obtained by subtracting the $P^+Q_A^-/PQ_A$ spectrum of RCs cooled in the dark from the corresponding spectrum of RCs cooled in the light. For wild-type RCs, some of the effects of freezing in the light are qualitatively similar to the effects of the R(L135)E mutation: the P^+ keto bands at 1703 and 1713 cm^{-1} move apart and become more equal in intensity (see Figure 4 and Table 2) and the phase-phonon bands become weaker. In addition, the ester carbonyl stretching band near 1750 cm^{-1} shifts about 2 cm^{-1} to lower energies, and a P^+ band at 1656 cm^{-1} increases in intensity. The 1656-cm^{-1} band probably reflects a perturbation of a protein carbonyl C═O stretching group.[66] The spectral effects observed upon cooling the RCs under illumination were fully reversible after warming the sample to room temperature and recooling in the dark.

Freezing under illumination affects the FTIR spectra of the R(L135)E and R(M164)E RCs in much the same manner as it

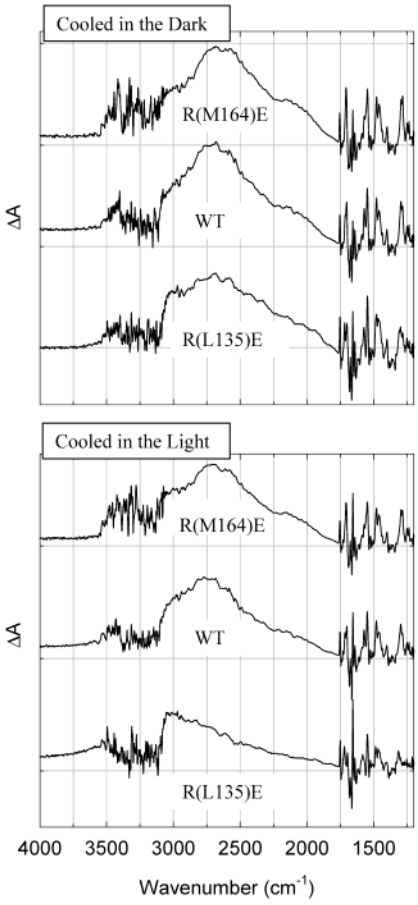

Figure 5. $P^+Q_A^-/PQ_A$ FTIR difference spectra in the range 4000−1200 cm^{-1} of RCs in hydrated films that were cooled to 100 K in the dark (top panel) or light (bottom).

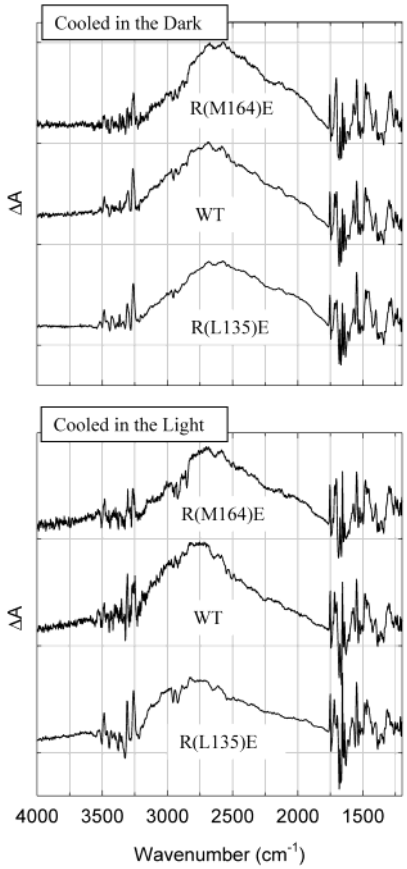

Figure 6. $P^+Q_A^-/PQ_A$ FTIR difference spectra in the range 4000−1200 cm^{-1} of RCs in "dry" films that were cooled to 100 K in the dark (top panel) or light (bottom).

affects wild-type RCs. The prominent band at 1656 cm^{-1}, the attenuation of the phase-phonon bands, and the small red-shift of the ester band are seen in both strains. The difference between the frequencies of the keto bands in the R(L135)E mutant, 18 cm^{-1} when the RCs are cooled in the dark, increases to 23 cm^{-1} after cooling in the light (Table 2). By contrast, illumination during cooling has little effect on the keto bands in the R(M164)E mutant. The attenuation of the phase-phonon bands and a shift of the 1295-cm^{-1} band to higher energy also are more pronounced in the R(L135)E mutant and in wild-type RCs than in the R(M164)E mutant. These effects are consistent with the picture that cooling under illumination results in further stabilization of the form of P^+ that predominates at room temperature. The relaxation should shift the spin distribution further in the direction of $|P_L^+\rangle$ in wild-type and R(L135)E RCs but stabilize a more even distribution of spin in the R(M164)E mutant.

Effects of the Mutations on the 2700 cm^{-1} Electronic Absorption Band of P^+. Figures 5 and 6 show light-induced FTIR difference spectra over a broader spectral range that includes the electronic absorption band of P^+ near 2700 cm^{-1}. The energy and dipole strength of this band are expected to depend on the energies of the basis states $|P_L^+\rangle$ and $|P_M^+\rangle$ and the coupling strength between these states.[17,19,24,25,31,32,71] The phase-phonon bands in the regions of 1290, 1480, and 1560 cm^{-1}, which as mentioned above represent vibrational modes that become allowed by coupling to the electronic transition, also can be seen in Figures 5 and 6. The 2700 cm^{-1} band and the phase-phonon bands are seen in RCs in which P is oxidized either photochemically, electrochemically, or chemically[72] but are not seen for monomeric Bchl cation in solution.[17,32] They are lost in heterodimer RCs, where the spin of P^+ locates essentially on the remaining Bchl.[17,32,73] The shape of the electronic band and the significance of the shoulder at 2200 cm^{-1} are not well understood, although, as discussed below, several investigators have attempted to model the coupling of the electronic and vibrational transitions.[19,25]

TABLE 3: Midpoint Potentials and FTIR Peak Energies in Wild-Type and Mutant RCs[a]

		ΔU_{peak} (cm^{-1})			
strain	ΔE_m (mV)	hydr, dark[b]	hydr, light[c]	dry, dark[d]	dry, light[e]
R(M164)E	−32	2680	2700	2650	2700
R(M164)L	−16	ND[f]	ND	ND	ND
WT	(0)	2680	2750	2690	2750
R(L135)L	−20	2680	ND	2650	2830
R(L135)E	−36	2680	>3000	2650	2840

[a] ΔE_m is the measured change in midpoint potential relative to wild-type RCs (from ref 43). The errors are ±5 mV. ΔU_{peak} is the energy corresponding to the measured absorption maximum of the electronic absorption band near 2700 cm^{-1}. [b] Hydrated films cooled in the dark. [c] Hydrated films cooled in the light. [d] "Dry" films cooled in the dark. [e] "Dry" films cooled in the light. [f] Not determined

Hydrated films of RCs cooled in the dark show only modest differences between the wild-type and mutant RC spectra in the 2700 cm^{-1} region (Figure 5, upper panel). The R(L135)E spectrum is broadened and has a smaller dipole strength, but the peak position is not changed significantly (see Table 3). Larger differences in the 2700 cm^{-1} band are seen if the RCs are illuminated during cooling (Figure 5, lower panel). In wild-type RCs, the peak shifts to higher frequencies by 70 cm^{-1}

compared to RCs that are cooled in the dark, as previously reported.[24] Such a shift would be expected if $|P_L^+\rangle$ is further stabilized relative to $|P_M^+\rangle$, increasing the energy difference between the ground and excited stationary states. The R(M164)E spectrum is downshifted by 50 cm^{-1} relative to the wild-type spectrum measured under the same conditions, and the R(L135)E spectrum now is shifted strongly to higher frequencies. The absorption maximum of the R(L135)E spectrum cannot be determined accurately because the spectrum is distorted by water absorption in the region above 3000 cm^{-1}.

To minimize interference by water absorption, samples also were prepared as "dry" films containing reduced amounts of water (Figure 6). When cooled in the light, these films also show the shifts of the 2700 cm^{-1} band to lower energy in the M164 mutant and higher energy in the L135 mutant: the band peaks at 2700 cm^{-1} in R(M164)E RCs, 2750 cm^{-1} in wild-type RCs, and 2840 cm^{-1} in R(L135)E (see Figure 6, lower panel, and Table 3). In the R(L135)L mutant, the peak is at 2830 cm^{-1} (not shown).

In the carbonyl region, the $P^+Q_A^-/PQ_A$ difference spectra of chromatophores from the strains containing the Leu or Glu mutation at L135 or M164 were similar to the spectra of purified RCs (not shown). However, the differences in the 2700 cm^{-1} band observed in the detergent-solubilized RCs were less apparent in the chromatophore spectra. The spectra of the purified RCs are emphasized above because they allow a more direct comparison to the Special TRIPLE measurements.

Discussion

The data presented above show that mutations of ionizable groups near P^+ can cause redistributions of electron spin between P_L and P_M. Mutations that replace Arg(L135) by a neutral or negatively charged group should stabilize $|P_L^+\rangle$ and both lower the E_m and increase the spin-distribution ratio; homologous mutations of Arg(M164) should stabilize $|P_M^+\rangle$, lower the E_m, and decrease ρ_L/ρ_M. The measured spin distributions and ΔE_m are qualitatively consistent with these expectations. Arginines L135 and M164 have no covalent or van der Waals interactions with the Bchls, and mutations of these residues appear not to alter the intramolecular spin distributions of the individual Bchls significantly (see the ratios R_L and R_M in Table 1), indicating that the molecular orbitals are largely unchanged.

Electronic Model and Electron−Phonon Coupling. To discuss the effects of the mutations on the 2700 cm^{-1} transition and the spin distribution in P^+ more quantitatively, it is useful to start with the simple model shown in Figure 7, which includes electronic, but not vibronic, coupling. The interaction Hamiltonian for this system is

$$\mathbf{H} = \begin{bmatrix} U_L & \beta \\ \beta & U_M \end{bmatrix} \tag{2}$$

where U_L and U_M are the energies of the diabatic states $|P_L^+\rangle$ and $|P_M^+\rangle$ and β is the electronic coupling strength. Diagonalization yields two eigenstates:

$$|\gamma_+\rangle = 2^{-1/2}(1+s)^{1/2}|P_L^+\rangle + 2^{-1/2}(1-s)^{1/2}|P_M^+\rangle$$
$$|\gamma_-\rangle = 2^{-1/2}(1-s)^{1/2}|P_L^+\rangle - 2^{-1/2}(1+s)^{1/2}|P_M^+\rangle \tag{3}$$

where $s = \delta/(\delta^2 + 4\beta^2)^{1/2}$ and $\delta = U_M - U_L$. The energies

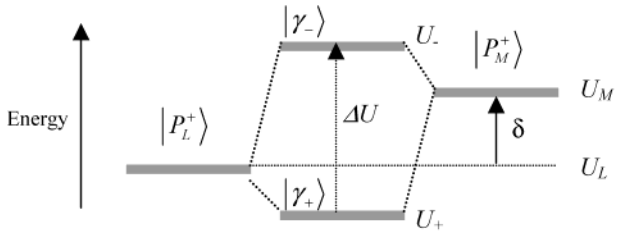

Figure 7. Two-state electronic model for P^+. U_L and U_M are the energies of the diabatic basis states $|P_L^+\rangle$ and $|P_M^+\rangle$. The difference between U_L and U_M (δ) and the electronic coupling of the basis states (β) determine the energies (U_+ and U_-) of the eigenstates ($|\gamma_+\rangle$ and $|\gamma_-\rangle$). ΔU is the electronic transition between the eigenstates. The midpoint potential (E_m) depends on the energy of the lower eigenstate.

of these states are given by

$$U_\pm = \frac{U_L + U_M}{2} \mp \frac{1}{2}\sqrt{\delta^2 + 4\beta^2} \tag{4}$$

Semiempirical molecular orbital calculations indicate that β is negative in this representation, making U_+ the lower eigenvalue.[17]

In this model, the midpoint potential of P/P^+ is given by

$$E_m = U_+/e + C \tag{5}$$

where e is the electron charge and C is a constant. The ratio of the net spins on P_L and P_M, which is obtained experimentally from the Special TRIPLE spectra as described above (eq 1), can be related to the ratio of the squares of the coefficients for $|P_L^+\rangle$ and $|P_M^+\rangle$ in the ground-state eigenfunction:

$$\frac{\rho_L}{\rho_M} = \frac{|\langle P_L^+|\gamma_+\rangle|^2}{|\langle P_M^+|\gamma_+\rangle|^2} = (\sqrt{x^2+1} + x)^2 \tag{6}$$

where $x = \delta/2|\beta|$. Rearranging this expression gives

$$\frac{\delta}{|\beta|} = 2x = \left(\frac{\rho_L}{\rho_M}\right)^{1/2} - \left(\frac{\rho_M}{\rho_L}\right)^{1/2} \tag{7}$$

The electronic model also provides the energy difference between the two eigenstates:

$$\Delta U = U_- - U_+ = \sqrt{\delta^2 + 4\beta^2} \tag{8}$$

The broad FTIR absorption band peaking near 2700 cm^{-1} is assigned to this excitation.[17]

Reimers et al.[22] and Müh et al.[23] have extended this model to include a semiclassical treatment of electron−phonon coupling. In this analysis, the energy difference between the diabatic states $|P_L^+\rangle$ and $|P_M^+\rangle$ in a given RC mutant (δ') depends on a set of normal coordinates (y_i) in addition to the electronic energy difference (δ):

$$\delta' = U_M - U_L + \sum_i 2k_i y_i D_i \tag{9}$$

where k_i and D_i are the force constant and displacement for vibrational mode i. The reorganization energy for mode i (λ_i) is $2k_iD_i^2$ and the total reorganization energy (λ) is

$$\lambda = \sum_i \lambda_i = \sum_i 2k_i D_i^2 \tag{10}$$

TABLE 4: Diabatic Energies and Transition Energies in a Model with Semiclassical Electron−Phonon Coupling[a] and Diabatic Energies Calculated Using a Distance-Dependent Screening Function[b]

strain	δ' (meV)	ΔU_{calc} (cm^{-1})	$\Delta\Delta V_L$ (meV)	$\Delta\Delta V_M$ (meV)
R(M164)E	41	2520	−27	−39
R(M164)L	74	2570	−15	−19
WT	118	(2680)	(0)	(0)
R(L135)L	173	2860	−26	−14
R(L135)E	185	2910	−56	−28

[a] The diabatic energy difference (δ') and the energy difference between the two eigenstates (ΔU) were calculated by eqs 11 and 12 with $\beta = -155$ meV. [b] The changes in the solvation energies of P_L^+ and P_M^+ relative to wild-type RCs ($\Delta\Delta V_L$ and $\Delta\Delta V_M$) were calculated by eqs 14 and 15 as described[43] with $\eta = 0.1$ Å^{-1} in eq 15. Five configurations of the polar hydrogens of the protein and crystallographic water molecules in each charge state of P were averaged for each strain of RCs. The standard error of the mean was ∼7 meV in all cases.

In this model, eqs 7 and 8 become

$$\frac{\delta'}{|\beta|} = \left(\frac{\rho_L}{\rho_M}\right)^{1/2} - \left(\frac{\rho_M}{\rho_L}\right)^{1/2} \tag{11}$$

and

$$\Delta U = \sqrt{\delta'^2 + 4\beta^2} \tag{12}$$

Müh et al.[23] have used this model to fit the changes in ρ_L/ρ_M and E_m for a large series of mutations of hydrogen-bonding residues. They assumed that mutations that alter the hydrogen bonding of P_L affect the energy of $|P_M^+\rangle$ by a constant fraction of the effects on $|P_L^+\rangle$ and vice versa. This gave values of 120−160 meV for $|\beta|$ and 100−200 meV for λ. Here, we take a somewhat different approach that makes use of the observed IR transition energy in WT RCs ($\Delta U \approx 2680$ cm^{-1}). Given this value and ρ_L/ρ_M (2.11), eqs 11 and 12 can be solved for δ' and β in WT RCs, yielding $\delta' = 118$ meV and $\beta = -155$ meV. Assuming again that the mutations do not alter β, the values of δ' for the R(L135)E, R(L135)L, R(M164)E, and R(M164)L mutants then can be obtained from the measured spin ratios by eq 11. The results are given in Table 4, along with the IR transition energies calculated by eq 12 (ΔU_{calc}).

The reorganization energy can be obtained by using the expression[22,88]

$$\rho_M^{\,2}\lambda = \mathcal{J}E_m + |\beta|\left(\frac{\rho_M}{\rho_L}\right)^{1/2} - U_L + C \tag{13}$$

where $\mathcal{J}$ is the Faraday constant and C is a constant. (The sign of the term $-U_L$ is opposite that of the corresponding term E_L in eq 11 of Reimers et al.[22] because of our different representation of the basis states.) To do this, we used the measured E_m and $(\rho_M/\rho_L)^{1/2}$ in the WT and mutant RCs and $|\beta| = 155$ meV from the fit to eqs 11 and 12 just described, and replaced U_L by the calculated electrostatic energy of oxidizing P_L in each strain (ΔV_L). The electrostatic energy was calculated with the expression

$$\Delta V_L = \sum_i (q_i^{P_L^+} - q_i^{P_L}) \sum_j q_j r_{ij}^{-1} f_{ij}^{-1} \tag{14}$$

Here $q_i^{P_L}$ and $q_i^{P_L^+}$ are the partial charges of atom i of P_L in the reduced and oxidized states, q_j is the charge of atom j of the protein, crystallographic water molecules, or other pigments, r_{ij} is the interatomic distance, and f_{ij} is a distance-dependent dielectric screening function. We used the screening function

$$f_{ij} = 1 + 60(1 - \exp(-\eta r_{ij})) \tag{15}$$

with $\eta = 0.1$ Å^{-1}, which has been found to reproduce measured electrostatic effects of ionizable groups on pK_a values and the E_m of P in the RC and other proteins.[43,74] We assumed that Arg and Glu at L135 and M164 are ionized, and we averaged the calculated energies over 10 configurations of the polar hydrogens for each bacterial strain and each state of P as described by Johnson and Parson.[43]

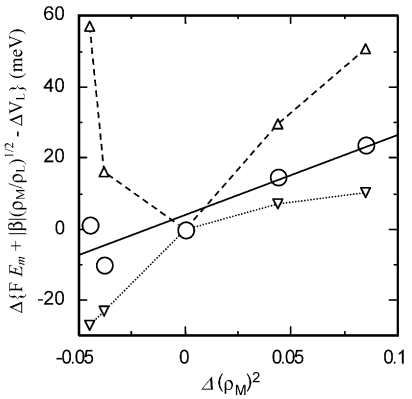

Figure 8. Changes in the quantity $\{\mathcal{J}E_m + |\beta|(\rho_M/\rho_L)^{1/2} - \Delta V_L\}$ in the mutant RCs relative to WT, plotted against the corresponding changes in ρ_M^2 (see eq 13). The changes in the energies of $|P_L^+\rangle$ (ΔV_L) were calculated using the screening parameter $\eta = 0.10$ Å^{-1} in eq 15 (○). The solid line shows a linear regression to these points; its slope gives $\lambda = 224$ meV. The upward triangles (△) and dashed line show the results of increasing ΔV_L by a factor of 2, and the downward triangles (▽) and dotted line show the results of decreasing ΔV_L by a factor of 2.

In Figure 8, the changes in the quantity on the right-hand side of eq 13 for the mutant RCs relative to WT ($\Delta\{\mathcal{J}E_m + |\beta|(\rho_M/\rho_L)^{1/2} - \Delta V_L\}$) are plotted against the changes in ρ_M^2 ($\Delta\{\rho_M^2\}$). A linear fit to the data yields a λ of 224 meV with a correlation coefficient of 0.93. This value of λ is within the range $0 < \lambda < 0.3$ eV suggested by Reimers and Hush[19,22,71] based on an analysis of the absorption spectrum but greater than the range of values that these authors favored based on an analysis of the hydrogen-bonding mutants ($0.1 < \lambda < 0.2$ eV).

It is important to note that the analysis described here depends on calculated values for ΔV_L and that such electrostatic calculations in proteins are subject to a variety of errors. However, the distance-dependent screening factor given by eq 15 appears to work well in both water-soluble and membrane proteins[43,74] and also appears to account satisfactorily for vibrational Stark effects on the keto vibrational frequencies in P_L^+ and P_M^+ (see below). To examine the sensitivity of the apparent value of λ to errors in the electrostatic calculations, the triangles in Figure 8 show the results of increasing or decreasing the calculated values of $\Delta\Delta V_L$ for all of the strains by a factor of 2. Linear fits to these data (not shown in Figure 8) yield $\lambda = 85$ and 294 meV with correlation coefficients of 0.20 and 0.94, respectively. We deem these fits to be unacceptable because of the systematic upward or downward curvatures of the plots. Our results would, however, be compatible with an increase in exponential factor η in eq 15 from 0.10 to 0.18 Å^{-1}, which would reduce the calculated values of $\Delta\Delta V_L$ slightly[43] and give a slightly larger value of λ.

A model with semiclassical electron−phonon coupling thus can give a self-consistent account of ρ_L/ρ_M and ΔE_m in the WT and mutant RCs and of the transition energy ΔU in WT RCs.

However, this analysis leaves several problems. First, the R(L135)E and R(M164)E mutations would be expected to change ΔU by 100−250 cm^{-1} (Table 4), which is larger than the observed shifts (Table 3). In addition, a more complete treatment will be needed in order to account adequately for the shape and dipole strength of the 2700 cm^{-1} absorption band. In the simple treatment used here, the dipole strength ($|\vec{\mu}|^2$) would be given by

$$\vec{\mu} = \langle \gamma_- | \tilde{\mu} | \gamma_+ \rangle = \frac{[(1+s)(1-s)]^{1/2}}{2} (\vec{r}_M - \vec{r}_L) e \qquad (16)$$

where $\vec{r}_M$ and $\vec{r}_L$ are the centers of electron density in P_M and P_L, e is the electronic charge, and $s = \delta'/(\delta'^2 + 4\beta^2)^{1/2}$. With the values of β and δ' suggested above, the predicted dipole strength for WT and all of the mutant RCs is about 300 D^2, which is considerably greater than the measured value of 25 D^2.[17] Reimers et al.[30] and Cave et al.[75] have suggested that the small dipole strength results from electron correlation effects that reduce the effective distance between the centers of $|P_L^+\rangle$ and $|P_M^+\rangle$.

Gasyna and Schatz[25] have used a non-Born−Oppenheimer treatment that includes strong coupling to a single low-frequency symmetric mode and weaker coupling to a high-frequency antisymmetric mode. They obtained a satisfactory fit to the 2700 cm^{-1} transition energy with $\delta = 37$ meV and $\beta = -60$ meV. However, the spin distribution between P_L and P_M was calculated before the vibronic interaction matrix was diagonalized. A reevaluation after the diagonalization results in a higher ρ_L/ρ_M that no longer agrees with the experimental value. More importantly, the calculated P^+ absorption spectrum includes strong bands below 2000 cm^{-1} that are not observed in the experimental spectrum. Reimers et al.[76] recently described a more successful treatment with a large number of explicit intramolecular modes, whose frequencies were obtained by density functional calculations on monomeric Bchl. Additional work will be needed to see whether a satisfactory account of all of the experimental observations can be obtained by incorporating protein modes in such a model.

Experimental Conditions and Protein Relaxations. In combining experimental results from ENDOR/TRIPLE and FTIR spectroscopy as we have done above, it is important to consider the differences between the conditions used for the two experiments. Although purified RCs in CHAPS detergent were used throughout, the FTIR measurements required hydrated or partially dehydrated films, whereas the TRIPLE spectra were recorded in solution. However, RCs probably remain well solvated in the films because, as shown in Figures 5 and 6, samples containing different amounts of water give similar spectra. Resonance Raman spectra of RCs in solution also are generally in good accord with FTIR spectra of films.[69] The E_m values used in the analysis were measured in solutions containing LDAO[43] but were found not to depend significantly on the choice of detergent (unpublished results).

A second difference is that the TRIPLE spectra were measured at 288 K, whereas the FTIR spectra were measured at 100 K. However, ENDOR/TRIPLE spectra of wild-type RCs have been measured previously over a wide range of temperatures, and the spin distribution ratio is relatively insensitive to the temperature.[27] Temperature also has relatively little effect on the FTIR spectra of wild-type RCs,[17] and we found that $P^+Q_A^-/PQ_A$ difference spectra of wild-type and mutant chromatophores at room temperature (not shown) were similar to those of purified RCs at 100 K.

Another difference is the anion present in the charge-separated state. $P^+Q_A^-/PQ_A$ difference spectra were obtained in the FTIR measurements because electron transfer to Q_B was inhibited by stigmatellin, whereas a combination of $P^+Q_A^-$ and $P^+Q_B^-$ probably was present in the Special TRIPLE measurements. The electrostatic environments of P^+ thus were slightly different in the two experiments. This difference seems unlikely to be of major importance, because the quinones are located relatively far from P. To our knowledge, there have been no reports of effects of Q_A^- or Q_B^- on the spin distribution or FTIR spectrum of P^+.

Perhaps most importantly, somewhat different protocols were used to generate P^+ for the TRIPLE and FTIR spectra. In the TRIPLE measurements, the sample was illuminated with saturating, continuous light at 288 K. These conditions allow the protein to relax around P^+, which could further stabilize $|P_L^+\rangle$ relative to $|P_M^+\rangle$ and make the spin distribution more asymmetric. In the FTIR measurements, the sample was exposed alternately to darkness and saturating light.

To explore the possible effects of protein relaxations on the FTIR difference spectra, we measured these spectra with RCs cooled either under continuous illumination or in the dark.The results presented in Figures 3−5 and Tables 2 and 3 show that the interactions of the protein with P^+ vary, depending on the freezing procedure. Most notably, illumination of wild-type RCs during cooling increases the splitting of the keto C═O vibrations of $|P_L^+\rangle$ and $|P_M^+\rangle$. The finding that the R(L135)E mutation also increases the splitting of these vibrations, whereas the R(M164)E mutation decreases it (Table 2), suggests that the splitting reflects an increased stabilization of $|P_L^+\rangle$ relative to $|P_M^+\rangle$. When RCs are cooled under illumination, the protein thus is likely to be trapped in a conformational state in which protein dipoles around P_L and P_M have relaxed to accommodate the distribution of the positive charge in P^+. This suggests that a significant component of the relaxation that slows the $P^+Q_A^-$ recombination kinetics in light-adapted samples[44−46] occurs around P^+. The shifts in the keto bands of $|P_L^+\rangle$ and $|P_M^+\rangle$ can be attributed to a vibrational Stark effect (see below).

Photovoltage measurements have shown that a charge is displaced along the transmembrane axis with a time constant of 200 μs following the formation of $P^+Q_A^-$.[77] These results were tentatively interpreted as reflecting either a movement of Q_A^- toward P^+ by about 2 Å or a change of the protonation states of residues near Q_A. However, no evidence for movements of the quinone was seen in Q_A^-/Q_A FTIR difference spectra,[78] or in magnetic resonance experiments.[79−81] The Q_A^-/Q_A FTIR difference spectra for RCs reconstituted with isotopically labeled ubiquinone, which are extremely sensitive to small changes in the interaction of the protein with Q_A and Q_A^-, are essentially the same in the presence of P at room temperature as in the presence of P^+ at low temperature.[78] The quinone marker bands also do not depend on whether the RCs are cooled to 100 K in the dark or under illumination (J. Breton, unpublished results). These observations are in accord with the suggestion that the change in the $P^+Q_A^-$ recombination kinetics upon cooling in the light stems mainly from reorganization of the protein around P^+ rather than Q_A^-.

A prominent feature at 1656/1664 cm^{-1} is associated with all of the $P^+Q_A^-/PQ_A$ FTIR difference spectra shown. This signal is enhanced when the RCs are cooled under illumination compared to samples cooled in the dark (Figures 3 and 4) and, like the splitting of the keto bands, is larger in the R(L135)E

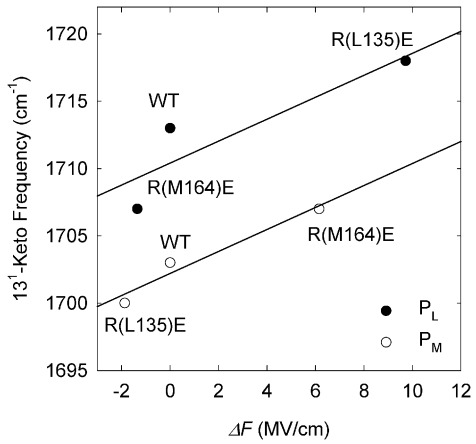

Figure 9. Measured 13^1-keto carbonyl frequencies for P_L^+ and P_M^+ in WT and mutant RCs cooled in the dark, as functions of the projection of the changes in the calculated electric field at the O atom along the C → O axis. The field was calculated using eqs 14 and 15 and was averaged for 10 configurations of the polar hydrogens of the protein and crystallographic water molecules relaxed around P in the reduced state. The points are labeled to indicate the RC strains. The errors in the calculated field and the measured frequency are indicated by the size of the symbol. The straight lines show linear regressions to the data.

mutant than in wild-type RCs. It also is dependent on the hydration state of the sample (E. Nabedryk and J. Breton, unpublished results). As discussed previously,[66] this signal could possibly reflect a conformational change of the protein backbone in response to the formation of P^+.

Vibrational Stark Effects. The effects of the R(L135)E and R(M164)E mutations on the keto C═O vibrational frequencies (Figure 3 and Table 2) can be attributed plausibly to vibrational Stark effects. Effects of this nature have been described previously for CO bound to the hemes in myoglobin and cytochrome *c* and for several carbonyl model compounds.[82−87] The "Stark tuning rate" is defined as $\delta_\nu = \partial\nu/\partial F$, where ν is the vibrational frequency and F is the projection of the local electric field ($\vec{F}$) on the C → O axis.[81] δ_ν depends on $-(\Delta\vec{\mu} + \vec{F}\cdot\Delta\bar{\alpha})\cdot\vec{F}$, where $\Delta\vec{\mu}$ is the difference between the dipole moments of the ground and excited vibrational states and $\Delta\bar{\alpha}$ is the corresponding difference in the polarizability tensor. For the keto vibrations in acetone, methyl vinyl ketone, and 1-methyl-2-pyrrolidinone, Park et al.[86] have measured Stark tuning rates of respectively $0.77/f$, $0.84/f$ and $1.17/f$ cm^{-1}/(MV/cm), where f is a local-field correction factor that probably is between 1 and 2.[87]

We calculated the electric fields at the 13^1-keto oxygen atoms of Bchls P_L and P_M with the expression

$$\vec{F}_i = \sum_j q_j |\vec{r}_{ij}|^{-2} f_{ij}^{-1} \hat{r}_{ij} \qquad (17)$$

Here $\vec{F}_i$ is the electric field at oxygen atom i, q_j is the charge of atom j of the protein or the other pigments, $\vec{r}_{ij}$ is the vector from atom j to atom i, $\hat{r}_{ij}$ is a unit vector parallel to $\vec{r}_{ij}$, and f_{ij} is the distance-dependent dielectric screening function of eq 15. The projection of the field on the C → O axis then is $F_i = \vec{F}_i\cdot\hat{b}_{co(i)}$, where $\hat{b}_{co(i)}$ is a unit vector along this axis. We assumed again that the Arg and Glu at L135 and M164 are ionized,[43] and we averaged the calculated field over 10 configurations of the polar hydrogens for each bacterial strain,[43] allowing the protein to relax around P for RCs cooled in the dark and around P^+ for RCs cooled in the light. Figure 9 shows the measured frequencies of the keto vibrations for P_L^+ and P_M^+ in RCs cooled in the dark (Table 2), as functions of the changes in the electric field (ΔF_i) calculated with the screening parameter $\eta = 0.10$ $Å^{-1}$ in eq 15. Linear fits to these data yield Stark tuning rates of 0.81 and 0.82 cm^{-1}/(MV/cm) for P_L^+ and P_M^+, respectively, with correlation coefficients of 0.89 and 0.98. Similar fits using $\eta = 0.18$ $Å^{-1}$ (not shown) gave tuning rates of 1.13 and 1.05 cm^{-1}/(MV/cm) with correlation coefficients of 0.91 and 0.99 for P_L^+ and P_M^+, respectively. Fits to the data for RCs cooled in the light (not shown) gave tuning rates of 0.83 and 1.12 cm^{-1}/(MV/cm) for P_L^+ and P_M^+, respectively, with $\eta = 0.1$ $Å^{-1}$, and 1.38 and 1.45 cm^{-1}/(MV/cm) with $\eta = 0.18$ $Å^{-1}$. Although no information is available on the Stark tuning rate for the 13^1-keto vibration of monomeric Bchl in solution, these results are similar to the tuning rates measured by Park et al.[87] for C═O stretching modes in other ketones.

When RCs are cooled in the light, the C═O vibration shifts to higher frequency in P_L and to lower frequency in P_M (Figure 4 and Table 2). If these shifts reflect Stark effects, the electric field along the C → O axis of P_L must increase, whereas that along the corresponding axis of P_M becomes more negative. These changes in local fields could be components of an overall increase in the field pointing from P_M to P_L, which would favor movement of positive charge in this direction. The shifts of the C═O vibration frequencies thus are consistent with the idea that relaxations of the protein stabilize P_L^+ relative to P_M^+. (The calculated value of F_i at the keto oxygen of P_L was always more negative than that at P_M. However, this difference probably is less reliable than the changes in F_i caused by the mutations because it is sensitive to short-range interactions that may not be treated accurately by the simple screening function used here.)

As noted above, the effects of the mutations on the keto vibration frequencies in P_L and P_M are smaller than the effects in P_L^+ and P_M^+. This suggests that oxidation of P increases either $\Delta\vec{\mu}$ or $\Delta\bar{\alpha}$. Alternatively, a change in the charge on P could increase $\vec{F}$ by modifying the ionization state of the residue at the mutation site.

Acknowledgment. This work was supported by National Science Foundation Grants MCB-9904618 and MCB-0131764, a Molecular Biophysics Training Grant (GM08268) from the National Institutes of Health, Sfb 498 (Deutsche Forschungsgemeinschaft), and Fonds der Chemischen Industrie (W.L.). We thank Dr. Steven Boxer for the pRKSCH/pHis vector, and Drs. Jeffrey Reimers, Noel Hush, Arieh Warshel, and V. Nagarajan and a reviewer for helpful comments and suggestions.

References and Notes

(1) Hoff, A. J.; Deisenhofer, J. *Phys. Reports* **1997**, *287*, 1.
(2) Deisenhofer, J.; Epp, O.; Miki, K.; Huber, R.; Michel, H. *J. Mol. Biol.* **1984**, *180*, 385.
(3) Allen, J. P.; Feher, G.; Yeates, T. O.; Komiya, H.; Rees, D. C. *Proc. Natl. Acad. Sci. U.S.A.* **1987**, *84*, 6162.
(4) El-Kabbani, O.; Chang, C. H.; Tiede, D.; Norris, J.; Schiffer, M. *Biochemistry* **1991**, *30*, 5361.
(5) Ermler, U.; Fritzsch, G.; Buchanan, S. K.; Michel, H. *Structure* **1994**, *2*, 925.
(6) Kirmaier, C.; Holten, D.; Parson, W. W. *Biochim. Biophys. Acta* **1985**, *810*, 33.
(7) Kirmaier, C.; Holten, D.; Parson, W. W. *Biochim. Biophys. Acta* **1985**, *810*, 49.
(8) Breton, J.; Martin, J.-L.; Migus, A.; Antonetti, A.; Orszag, A. *Proc. Natl. Acad. Sci. U.S.A.* **1986**, *83*, 5121.
(9) Lockhart, D. J.; Kirmaier, C.; Holten, D.; Boxer, S. G. *J. Phys. Chem.* **1990**, *94*, 6987.
(10) Heller, B. A.; Holten, D.; Kirmaier, C. *Science* **1995**, *269*, 940.
(11) Kirmaier, C.; He, C.; Holten, D. *Biochemistry* **2001**, *40*, 12132.
(12) Robles, S. J.; Breton, J.; Youvan, D. C. *Science* **1990**, *248*, 1402.

(13) Taguchi, A. K.; Stocker, J. W.; Alden, R. G.; Causgrove, T. P.; Peloquin, J. M.; Boxer, S. G.; Woodbury, N. W. *Biochemistry* **1992**, *31*, 10345.
(14) Alden, R. G.; Parson, W. W.; Chu, Z. T.; Warshel, A. *J. Am. Chem. Soc.* **1995**, *117*, 12284.
(15) Gunner, M.; Nichols, A.; Honig, B. *J. Phys. Chem.* **1996**, *100*, 4277.
(16) Parson, W. W.; Chu, Z. T.; Warshel, A. *Biochim. Biophys. Acta* **1990**, *1017*, 251.
(17) Breton, J.; Nabedryk, E.; Parson, W. W. *Biochemistry* **1992**, *31*, 7503.
(18) Plato, M.; Lendzian, F.; Lubitz, W.; Möbius, K. In *The Photosynthetic Bacterial Reaction Center II Structure, Spectroscopy, and Dynamics*; Breton, J., Vermeglio, A., Eds.; Plenum Press: New York, 1992; p 109.
(19) Reimers, J. R.; Hush, N. S. *Chem. Phys.* **1995**, *197*, 323.
(20) Reimers, J. R.; Hush, N. S. *J. Am. Chem. Soc.* **1995**, *117*, 1302.
(21) Artz, K.; Williams, J. C.; Allen, J. P.; Lendzian, F.; Rautter, J.; Lubitz, W. *Proc. Natl. Acad. Sci. U.S.A.* **1997**, *94*, 13582.
(22) Reimers, J. R.; Hughes, J. M.; Hush, N. S. *Biochemistry* **2000**, *39*, 16185.
(23) Müh, F.; Lendzian, F.; Roy, M.; Williams, J. C.; Allen, J. P.; Lubitz, W. *J. Phys. Chem. B* **2002**, *106*, 3226.
(24) Parson, W. W.; Nabedryk, E.; Breton, J. In *The Photosynthetic Bacterial Reaction Center II Structure Spectroscopy, and Dynamics*; Breton, J., Vermeglio, A., Eds.; Plenum Press: New York, 1992; p 79.
(25) Gasyna, Z.; Schatz, P. N. *J. Phys. Chem.* **1996**, *100*, 1445.
(26) Lendzian, F.; Huber, M.; Isaacson, R. A.; Endeward, B.; Plato, M.; Bönigk, B.; Möbius, K.; Lubitz, W.; Feher, G. *Biochim. Biophys. Acta* **1993**, *1183*, 139.
(27) Rautter, J.; Lendzian, F.; Wang, S.; Allen, J. P.; Lubitz, W. *Biochemistry* **1994**, *33*, 12077.
(28) Rautter, J.; Lendzian, F.; Schulz, C.; Fetsch, A.; Kuhn, M.; Lin, X.; Williams, J. C.; Allen, J. P.; Lubitz, W. *Biochemistry* **1995**, *34*, 8130.
(29) Plato, M.; Krauss, N.; Fromme, P.; Lubitz, W. *Biochim. Biophys. Acta* **2002**, submitted.
(30) Reimers, J. R.; Hutter, M. C.; Hughes, J. M.; Hush, N. S. *Int. J. Quantum Chem.* **2000**, *80*, 1224.
(31) Breton, J.; Nabedryk, E.; Clerici, A. *Vib. Spectrosc.* **1999**, *19*, 71.
(32) Nabedryk, E.; Schulz, C.; Müh, F.; Lubitz, W.; Breton, J. *Photochem. Photobiol.* **2000**, *71*, 582.
(33) Williams, J. C.; Alden, R. G.; Murchison, H. A.; Peloquin, J. M.; Woodbury, N. W.; Allen, J. P. *Biochemistry* **1992**, *31*, 11029.
(34) Hynninen, P. H. Chemistry of Chlorophylls: Modifications. In *Chlorophylls*; Scheer, H., Ed.; CRC Press: Boca Raton, FL, 1991; p 145.
(35) Allen, J. P.; Artz, K.; Lin, X.; Williams, J. C.; Ivancich, A.; Albouy, D.; Mattioli, T. A.; Fetsch, A.; Kuhn, M.; Lubitz, W. *Biochemistry* **1996**, *35*, 6612.
(36) Murchison, H. A.; Alden, R. G.; Allen, J. P.; Peloquin, J. M.; Taguchi, A. K.; Woodbury, N. W.; Williams, J. C. *Biochemistry* **1993**, *32*, 3498.
(37) Spiedel, D.; Roszak, A. W.; McKendryck, K.; McAuley, K. E.; Fyfe, P. K.; Nabedryk, E.; Breton, J.; Robert, B.; Cogdell, R. J.; Isaacs, N. W.; Jones, M. R. *Biochim. Biophys. Acta* **2002**, *1554*, 75.
(38) Lin, X.; Murchison, H. A.; Nagarajan, V.; Parson, W. W.; Allen, J. P.; Williams, J. C. *Proc. Natl. Acad. Sci. U.S.A.* **1994**, *91*, 10265.
(39) Wachtveitl, J.; Farchaus, J. W.; Das, R.; Lutz, M.; Robert, B.; Mattioli, T. A. *Biochemistry* **1993**, *32*, 12875.
(40) Müh, F.; Schulz, C.; Schlodder, E.; Jones, M. R.; Rautter, J.; Kuhn, M.; Lubitz, W. *Photosynth. Res.* **1998**, *55*, 199.
(41) Müh, F.; Bibikova, M.; Lendzian, F.; Oesterhelt, D.; Lubitz, W. In *Photosynthesis: Mechanisms and Effects*; Garab, G., Ed.; Kluwer: Dordrecht, 1998; Vol. 2; p 763.
(42) Kuglstatter, A.; Hellwig, P.; Fritzsch, G.; Wachtveitl, J.; Oesterhelt, D.; Mäntele, W.; Michel, H. *FEBS Lett* **1999**, *463*, 169.
(43) Johnson, E. T.; Parson, W. W. *Biochemistry* **2002**, *41*, 6483.
(44) Kleinfeld, D.; Okamura, M. Y.; Feher, G. *Biochemistry* **1984**, *23*, 5780.
(45) McMahon, B. H.; Muller, J. D.; Wraight, C. A.; Nienhaus, G. U. *Biophys. J.* **1998**, *74*, 2567.
(46) Xu, Q.; Gunner, M. R. *Biochemistry* **2001**, *40*, 3232.
(47) Paddock, M. L.; Rongey, S. H.; Feher, G.; Okamura, M. Y. *Proc. Natl. Acad. Sci. U.S.A.* **1989**, *86*, 6602.
(48) Lin, X.; Williams, J. C.; Allen, J. P.; Mathis, P. *Biochemistry* **1994**, *33*, 13517.
(49) Goldsmith, J. O.; Boxer, S. G. *Biochim. Biophys. Acta* **1996**, *1276*, 171.
(50) Feher, G.; Okamura, M. Y. In *The Photosynthetic Bacteria*; Clayton, R. K., Sistrom, W. R., Eds.; Plenum Press: New York, 1978; p 349.
(51) Müh, F.; Rautter, J.; Lubitz, W. *Biochemistry* **1997**, *36*, 4155.
(52) Tränkle, E.; Lendzian, F. *J. Magn. Reson.* **1989**, *84*, 537.
(53) Nabedryk, E.; Allen, J. P.; Taguchi, A. K.; Williams, J. C.; Woodbury, N. W.; Breton, J. *Biochemistry* **1993**, *32*, 13879.
(54) Nabedryk, E.; Breton, J.; Williams, J. C.; Allen, J. P.; Kuhn, M.; Lubitz, W. *Spectrochim. Acta A* **1998**, *54*, 1219.
(55) Stowell, M. H.; McPhillips, T. M.; Rees, D. C.; Soltis, S. M.; Abresch, E.; Feher, G. *Science* **1997**, *276*, 812.
(56) Nabedryk, E.; Bagley, K. A.; Thibodeau, D. L.; Bauscher, M.; Mäntele, W.; Breton, J. *FEBS Lett* **1990**, *266*, 59.
(57) Norris, J. R.; Katz, J. J. In *The Photosynthetic Bacteria*; Clayton, R. K., Sistrom, W. R., Eds.; Plenum Press: New York, 1978; p 397.
(58) Feher, G.; Hoff, A. J.; Isaacson, R. A.; Ackerson, L. C. *Ann. N. Y. Acad. Sci.* **1975**, *244*, 239.
(59) Norris, J. R.; Scheer, H.; Katz, J. J. *Ann. N. Y. Acad. Sci.* **1975**, *244*, 260.
(60) McConnell, H. M. *J. Chem. Phys.* **1956**, *24*, 632.
(61) Atherton, N. M. *Principles of Electron Spin Resonance*; Ellis Horwood PTR Prentice Hall: New York, 1993.
(62) Huber, M.; Isaacson, R. A.; Abresch, E. C.; Gaul, D.; Schenck, C. C. *Biochim. Biophys. Acta* **1996**, *1273*, 108.
(63) Mäntele, W.; Wollenweber, A.; Nabedryk, E.; Breton, J.; Rashwan, F.; Heinze, J.; Kreutz, W. In *Progress in Photosynthesis Research*; Biggins, J., Ed.; Martinus Nijhoff: Dordrecht, 1987; Vol. 1; p 329.
(64) Mäntele, W.; Wollenweber, A.; Nabedryk, E.; Breton, J. *Proc. Natl. Acad. Sci. U.S.A.* **1988**, *85*, 8468.
(65) Nabedryk, E.; Breton, J.; Wachtveitl, J.; Gray, K. A.; Oesterhelt, D. In *The Photosynthetic Bacterial Reaction Center II Structure, Spectroscopy, and Dynamics*; Breton, J., Vermeglio, A., Eds.; Plenum Press: New York, 1992; p 147.
(66) Nabedryk, E. In *Infrared Spectroscopy of Biomolecules*; Mantsch, H. H., Chapman, D., Eds.; Wiley-Liss: New York, 1996; p 39.
(67) Nabedryk, E.; Breton, J.; Allen, J. P.; Murchison, H. A.; Taguchi, A. K.; Williams, J. C.; Woodbury, N. W. In *The Photosynthetic Bacterial Reaction Center II Structure, Spectroscopy, and Dynamics*; Breton, J., Vermeglio, A., Eds.; Plenum Press: New York, 1992; p 141.
(68) Leonhard, M.; Mäntele, W. *Biochemistry* **1993**, *32*, 4532.
(69) Mattioli, T. A.; Williams, J. C.; Allen, J. P.; Robert, B. *Biochemistry* **1994**, *33*, 1636.
(70) Breton, J.; Nabedryk, E. *Chem. Phys. Lett.* **1993**, *213*, 571.
(71) Reimers, J. R.; Hush, N. S. *Chem. Phys.* **1996**, *208*, 177.
(72) Iwaki, M.; Andrianambinintsoa, S.; Rich, P. R.; Breton, J. *Spectrochim. Acta A* **2002**, *58*, 1523.
(73) Nabedryk, E.; Robles, S. J.; Goldman, E.; Youvan, D. C.; Breton, J. *Biochemistry* **1992**, *31*, 10852.
(74) Warshel, A.; Russell, S. T.; Churg, A. K. *Proc. Natl. Acad. Sci. U.S.A.* **1984**, *81*, 4785.
(75) Cave, R. J.; Newton, M. D. *Chem. Phys. Lett.* **1996**, *249*, 15.
(76) Reimers, J. R.; Rendell, A. P.; Hush, N. S. *PS2001 Proceedings* **2001**, www.publish.csiro.au/ps2001.
(77) Brzezinski, P.; Okamura, M. Y.; Feher, G. In *The Photosynthetic Bacterial Reaction Center II Structure, Spectroscopy and Dynamics*; Breton, J., Vermeglio, A., Eds.; Plenum Press: New York, 1992; p 321.
(78) Breton, J.; Boullais, C.; Burie, J. R.; Nabedryk, E.; Mioskowski, C. *Biochemistry* **1994**, *33*, 14378.
(79) van den Brink, J. S.; Hulsebosch, R. J.; Gast, P.; Hore, P. J.; Hoff, A. J. *Biochemistry* **1994**, *33*, 13668.
(80) Zech, S. G.; Bittl, R.; Gardiner, A. T.; Lubitz, W. *Appl. Magn. Reson.* **1997**, *13*, 517.
(81) Borovykh, I. V.; Dzuba, S. A.; Proskuryakov, I. I.; Gast, P.; Hoff, A. J. *Biochim. Biophys. Acta* **1998**, *1363*, 182.
(82) Lambert, D. K. *J. Chem. Phys.* **1988**, *89*, 3847.
(83) Chattopadhyay, A.; Boxer, S. G. *J. Am. Chem. Soc.* **1995**, *117*, 1449.
(84) Laberge, M.; Vanderkooi, J. M.; Sharp, K. A. *J. Phys. Chem.* **1996**, *100*, 10793.
(85) Phillips, G. N.; Teodoro, M.; Li, T.; Smith, B.; Gilson, M. M.; Olson, J. S. *J. Phys. Chem.* **1999**, *103*, 8817.
(86) Park, E. S.; Andrews, S. S.; Hu, R. B.; Boxer, S. G. *J. Phys. Chem. B* **1999**, *103*, 9813.
(87) Park, E. S.; Boxer, S. G. *J. Phys. Chem. B* **2002**, *106*, 5800.
(88) Equation 13 is strictly correct only if $\delta \gg 0$. However, for $|\beta| \approx 155$ and $\lambda \approx 200$ meV, it holds to within 0.2 meV for δ as small as 18 meV (the smallest value of δ for the mutants studied here).